

Synthesis and Characterization of Au-Loaded Core/Shell Mesoporous Silica Spheres Containing Propyl Group in the Shell

Hitoshi Kumagi* and Kazuhisa Yano

Toyota Central R & D Laboratories, Inc., 41-1 Nagakute, Aichi 480-1192, Japan

Received April 19, 2010. Revised Manuscript Received July 15, 2010

A series of organically functionalized core/shell monodispersed mesoporous silica spheres (MMSSs) containing bulky propyl group in the shell and thiol group as coordination sites of Au ions in the core were prepared. The thickness and molar ratio of propyl group in the shell are systematically controlled by changing the amount and composition of additional silica precursor. The core/shell MMSSs were converted to monodispersed gold-nanoparticle-embedded nanoporous spheres. It is found that the propyl group in the shell acts as a barrier to prevent the migration of gold nanoparticles. Gold nanoparticles are retained within the core after heat treatment, because of the steric hindrance and hydrophobic character of the propyl group. The absorption band of the gold nanoparticles showed blue-shift not only with decreasing thickness of the shell but also with increasing reduction temperature.

Introduction

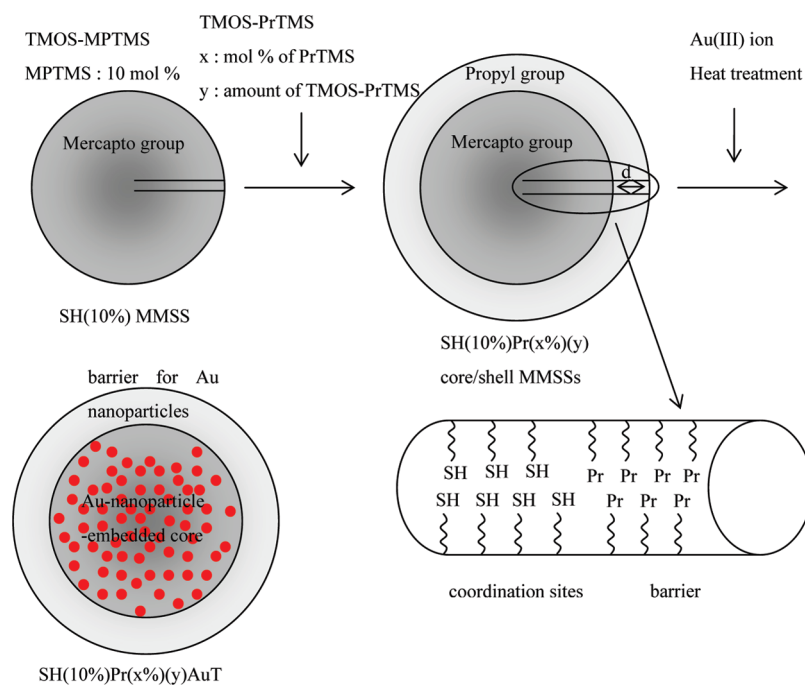
Mesoporous silica have attracted significant attention, because of their unique structures, such as their high specific surface areas, controllable pore structures, and narrow pore size distributions.^{1–3} The wide interest in these materials is driven by their emergence of physical and/or chemical properties, such as magnetism,^{4–6} optical properties,^{7–10} catalysis,^{11–13} adsorptivity^{14,15} and other potential technological applications. Controlling the morphologies of these materials is one of the major challenges that must be solved to enable their use in industrial applications. Among various shapes of particles,

spheres are of great interest for applications in separating molecules, catalysis, sensors, and colloidal crystals.^{16–20} Nonporous monodispersed silica spheres in the micrometer-sized range were first synthesized in 1968 by Stöber, who employed a system of water, alcohol, ammonia, and tetraalkoxysilane.²¹ We have succeeded in the synthesis of highly monodispersed mesoporous silica spheres (denoted as MMSSs hereafter) that contain ordered starburst (radially aligned) mesopores with hexagonal regularity from tetramethoxysilane and *n*-alkyltrimethylammonium bromide (C_nTMABr).^{22,23} The radially aligned and highly ordered mesopores of MMSSs offer high accessibility to guest molecules, which enables us to fabricate nanocomposite spheres with various types of functional materials such as organic dyes, metal oxides, and conducting polymers. We have been trying to develop MMSSs that exhibit physical or chemical properties, such as magnetic,^{4,5} optical,^{7,8} and catalytic properties.^{11,24–26} We have made a first step toward the practical use of MMSSs as magnetic or optical materials by incorporating inorganic particles or organic functional molecules in the mesopore. We have also synthesized core/shell MMSSs and shown their

- *
(1) Hoffmann, F.; Cornelius, M.; Morell, J.; Froba, M. *Angew. Chem., Int. Ed.* **2006**, *45*, 3216.
(2) Taguchi, A.; Schuth, F. *Microporous Mesoporous Mater.* **2005**, *77*, 1.
(3) Sayari, A. *Chem. Mater.* **1996**, *8*, 1840.
(4) Mizutani, M.; Yamada, Y.; Nakamura, T.; Yano, K. *Chem. Mater.* **2008**, *20*, 4777.
(5) Nakamura, T.; Yamada, Y.; Yano, K. *J. Mater. Chem.* **2006**, *16*, 2417.
(6) Froba, M.; Kohn, R.; Bouffaud, G.; Richard, O.; van Tendeloo, G. *Chem. Mater.* **1999**, *11*, 2858.
(7) Yamada, Y.; Yamada, H.; Nakamura, T.; Yano, K. *Langmuir* **2009**, *25*, 13599.
(8) Yamada, H.; Nakamura, T.; Yamada, Y.; Yano, K. *Adv. Mater.* **2009**, *21*, 4134.
(9) Lebeau, B.; Fowler, C. E.; Mann, S.; Farcet, C.; Charleux, B.; Sanchez, C. *J. Mater. Chem.* **2000**, *10*, 2105.
(10) Moller, K.; Bein, T. *Chem. Mater.* **1998**, *10*, 2950.
(11) Suzuki, T. M.; Nakamura, T.; Sudo, E.; Akimoto, Y.; Yano, K. *Microporous Mesoporous Mater.* **2008**, *111*, 350.
(12) Reynhardt, J. P. K.; Yang, Y.; Sayari, A.; Alper, H. *Chem. Mater.* **2004**, *16*, 4095.
(13) Maschmeyer, T.; Rey, F.; Sankar, G.; Thomas, J. M. *Nature* **1995**, *378*, 159.
(14) Antochshuk, V.; Olkhovyk, O.; Jaroniec, M.; Park, I. S.; Ryoo, R. *Langmuir* **2003**, *19*, 3031.
(15) Kang, T.; Park, Y.; Choi, K.; Lee, J. S.; Yi, J. J. *J. Mater. Chem.* **2004**, *14*, 1043.

- (16) Huo, Q.; Feng, J.; Schuth, F.; Stucky, G. *Chem. Mater.* **1997**, *9*, 14.
(17) Lin, H.-P.; Cheng, Y.-R.; Mou, C.-Y. *Chem. Mater.* **1998**, *10*, 3772.
(18) Qi, L.; Ma, J.; Cheng, H.; Zhao, Z. *Chem. Mater.* **1998**, *10*, 1623.
(19) Yano, K.; Fukushima, Y. *J. Mater. Chem.* **2004**, *14*, 1579.
(20) Wang, Y.; Price, A. D.; Caruso, F. *J. Mater. Chem.* **2009**, *19*, 6451.
(21) Stöber, W.; Fink, A.; Bohm, E. *J. Colloid Interface Sci.* **1968**, *26*, 62.
(22) Yano, K.; Fukushima, Y. *J. Mater. Chem.* **2003**, *13*, 2577.
(23) Yano, K.; Fukushima, Y. *J. Chem. Soc. Jpn.* **2003**, *76*, 2103.
(24) Suzuki, T. M.; Nakamura, T.; Akimoto, Y.; Yano, K. *Chem. Lett.* **2008**, *37*, 124.
(25) Suzuki, T. M.; Nakamura, T.; Fukumoto, K.; Yamamoto, M.; Akimoto, Y.; Akimoto, Y.; Yano, K. *J. Mol. Catal. A—Chem.* **2008**, *280*, 224.
(26) Suzuki, T. M.; Nakamura, T.; Sudo, E.; Akimoto, Y.; Yano, K. *J. Catal.* **2008**, *258*, 265.

Scheme 1. Schematic Illustration of the Core/Shell MMSS Having a Thiol Group in the Core and a Propyl Group in the Shell



catalytic activity, and we have clarified the important role of the shell. The catalytic activity is dependent not only on the pore size of MMSSs but also on the thickness of the shell.²⁶

Gold particles are very attractive for different reasons.^{27–29} For instance, they are ideal electrodes for molecular electronics. Gold clusters deposited onto thin metal oxides also exhibit unexpected high catalytic activity (not obtained with bulk metal) for different reactions, from combustion to hydrogenation and reduction. The optical properties such as surface plasmon resonance (SPR) and surface-enhanced Raman scattering (SERS) of gold nanoparticles have been extensively studied.³⁰ To stabilize gold nanoparticles, they were attached on silica surface and covered by mesoporous silica.³¹ For our continuing interests in making functional MMSSs, we have made use of gold particles as guest materials. We have reported on the direct synthesis of thiol-functionalized MMSSs and their application to gold-nanoparticle-embedded MMSSs.³² Most of the gold particles were confined inside the silica spheres. However, some of the gold particles were found on the outer surface. It is important to hold all of the gold particles inside the mesopore of silica spheres for many applications such as drug delivery, catalysis, and optical application. To expand our chemistry, we designed a series of core/shell MMSSs in which a thiol group is present in the core and a propyl group is present in the shell. The thiol group plays an essential role for the adsorption of AuCl_4^- ions in the core, and the propyl

group acts as a barrier to keep the gold particles inside the core, via steric hindrance and hydrophobic character. Here, we report the synthesis and characterization of a series of gold-nanoparticle-embedded core/shell MMSSs.

Experimental Section

Tetramethoxysilane (TMOS, Tokyo Kasei), mercaptopropyl trimethoxysilane, (MPTMS, Aldrich), propyl trimethoxysilane, (PrTMS, Aldrich), hydrogen tetrachloroaurate (Aldrich), hexadecyl trimethylammonium chloride (C_{16} -TMACl, Tokyo Kasei), 1 M sodium hydroxide solution (Wako, Inc.), methanol (Wako, Inc.), ethanol (Wako, Inc.), and concentrated hydrochloric acid (Wako, Inc.) were used without further purification.

Synthesis. Core/shell MMSSs were prepared according to the modified procedure reported in the previous paper.³³ For example, 3.52 g of C_{16} -TMACl and 2.28 mL of 1 M sodium hydroxide solution were dissolved in 800 g of methanol/water (50/50 = w/w) solution. Then, 1.19 g of TMOS and 0.17 g of MPTMS, which had been mixed under a dry nitrogen atmosphere, were added to the solution with vigorous stirring at 25 °C. The clear solution turned opaque in several minutes after the addition of the silica source and resulted in a white precipitate. After 1 h of continuous stirring, 1.14 mL of 1 M sodium hydroxide solution and 0.66 g of TMOS–PrTMS mixture were added to the suspension. After 8 h of continuous stirring, the mixture was aged overnight. The precipitate was then filtered off, washed with distilled water three times, and dried at 70 °C for 72 h. An acid extraction was performed in an ethanol (100 mL) mixture of concentrated hydrochloric acid (1.0 mL) and as-made materials (1.0 g) at 60 °C for 3 h. The surfactant-removed samples were filtered off, washed with ethanol, and dried in air. The amount of TMOS (1.19 g)–MPTMS (0.17 g) mixture for the synthesis of core is fixed and the additional amount and PrTMS ratio (expressed in terms of mol %) of TMOS–PrTMS mixture are systematically changed for other core/shell MMSSs.

(27) Chen, M. S.; Goodman, D. W. *Acc. Chem. Res.* **2006**, *39*, 739.

(28) Daniel, M. C.; Astruc, D. *Chem. Rev.* **2004**, *104*, 293.

(29) Jain, P. K.; Huang, X. H.; El-Sayed, I. H.; El-Sayed, M. A. *Acc. Chem. Res.* **2008**, *41*, 1578.

(30) Ghosh, S. K.; Pal, T. *Chem. Rev.* **2007**, *107*, 4797.

(31) Ge, J.; Zhang, Q.; Zhang, T.; Yin, Y. *Angew. Chem., Int. Ed. Engl.* **2008**, *47*, 8924.

(32) Nakamura, T.; Yamada, Y.; Yano, K. *J. Mater. Chem.* **2007**, *17*, 3726.

(33) Nakamura, T.; Mizutani, M.; Nozaki, H.; Suzuki, N.; Yano, K. *J. Phys. Chem. C* **2007**, *111*, 1093.

Table 1. Properties of a Series of SH(10%)Pr(x%)(y)

sample	shell/core ratio ^a	average particle size (nm)	standard deviation	pore size (nm)	specific surface area (m ² /g)	pore volume (mL/g)
SH(10%)Pr(0%)(1)	1	634	2.9	2.2	1302	0.74
SH(10%)Pr(10%)(1)	1	471	5.6	1.8	1426	0.65
SH(10%)Pr(25%)(1)	1	695	2.7	1.7	1377	0.58
SH(10%)Pr(50%)(1)	1	628	2.3	1.8	1273	0.40
SH(10%)Pr(75%)(1)	1	652	2.1	2.4	44	0.03
SH(10%)Pr(100%)(1)	1	620	4.1	2.5	5	0
SH(10%)Pr(50%)(3/4)	0.75	588	2.4	1.9	1105	0.54
SH(10%)Pr(50%)(1/2)	0.5	552	2.4	1.9	1203	0.65
SH(10%)Pr(50%)(1/4)	0.25	517	2.8	2.1	1269	0.66
SH(10%)Pr(75%)(1/2)	0.5	557	2.1	2.1	877	0.46
SH(10%)Pr(75%)(1/4)	0.25	503	2.5	1.7	1127	0.49
SH(10%)Pr(100%)(1/4)	0.25	467	1.9	1.9	887	0.42

^a Molar ratio of silica precursors used for the shell and core portion.

(See Scheme 1.) The resultant products are designated as SH-(10%)Pr(x%)(y), where SH(10%) indicates amount of MPTMS in the TMOS–MPTMS mixture in the core synthesis (in mol %), *x* shows the amount of PrTMS in the additional TMOS–PrTMS mixture (in mol %), and *y* shows the amount of TMOS–PrTMS for the shell (*y* = 1, 1/2, and 1/4 for 1.32 g of TMOS–PrTMS, 0.66 g of TMOS–PrTMS, and 0.33 g of TMOS–PrTMS, respectively).

In the encapsulation synthesis of gold nanoparticles, 0.5 g of SH(10%)Pr(x%)(y) was first added to an aqueous solution containing 0.3 g of HAuCl₄ solution (Aldrich, 30 wt % solution in dilute hydrochloric acid). After the mixture was stirred at room temperature for 10 min, the solid sample was filtered off and washed repeatedly with copious amounts of hydrochloric acid solution of pH 2 to remove the AuCl₄⁻ that had been adsorbed on the outer surfaces until the filtrate turned colorless and clear. The treated SH(10%)Pr(x%)(y)Au was annealed for 6 h in a 5% H₂–N₂ flow to form gold-nanoparticle-embedded spheres at different temperatures. The resultant products are designated as SH(10%)Pr(x%)(y)Au_T, where *T* indicates the annealing temperature.

Characterization. The particle morphology and the elemental composition were determined with a scanning electron microscopy (SEM) system that was equipped with an energy-dispersive X-ray (EDX) detector (Hitachi High-Technologies Corporation, Model S-3600N) at an acceleration voltage of 15 kV. The surface of the sample was coated with gold prior to the observation. The average particle size was calculated from the diameters of more than 50 particles in SEM images. Only parts of the SEM images are shown in the figures; particles not appearing in the figures were also examined. Transmission electron microscopy (TEM) micrographs were obtained with a Model JEOL-200CX TEM system using an acceleration voltage of 200 kV. The nitrogen adsorption isotherm was measured using a Belsorp-mini II (BEL Japan) system at 77 K. The sample was evacuated at 373 K under 10⁻³ mmHg before measurement. The pore diameter was calculated using the Barrett–Joyner–Halenda (BJH) method. The specific surface area was calculated using the Brunauer–Emmett–Teller (BET) plot for the adsorption branch. X-ray diffraction (XRD) measurement was performed with a Rigaku Model Rint-TTR X-ray diffractometer, using Cu radiation. The absorption spectrum was measured using a JASCO Model V-560 spectrophotometer.

Results and Discussion

Synthesis of Core/Shell MMSSs Having Different Shell Compositions. MMSSs are synthesized from TMOS and a surfactant under very specific conditions. In our previous

paper, the mechanism for the particle growth of a MMSS was proposed from the results of *in situ* TEM observation and XRD measurements. We have applied the formation mechanism for a MMSS to obtain highly monodispersed core/shell mesoporous silica spheres possessing a hydrophilic core and a hydrophobic shell.^{33,34} It is expected from the reported mechanism that the thickness of the shell and chemical properties such as hydrophobic (or hydrophilic) steric hindrance and coordination site of metal ions could be introduced and controlled by varying the silica precursor. To create a barrier in the shell, the propyl group, the size of which is appropriate for entry of the gold precursor as well as hindrance to the migration of gold nanoparticles, is introduced. Syntheses were conducted in which a mixture of TMOS and PrTMS was further added to a solution, including particles obtained from TMOS containing 10 mol % of MPTMS. This reaction gives core/shell MMSSs that have a thiol group in the core and a propyl group in the shell. (See Scheme 1.) The amount of propyl groups and the thickness of the shell are tuned by changing the amount and ratio of the TMOS–PrTMS mixture. SEM analysis yields important information about morphology of the particles. Figure S1 in the Supporting Information shows SEM images of a series of core/shell particles. The diameters of the particles have increased depending on the amount of TMOS–PrTMS mixture added, while retaining their monodispersed characteristics (see Table 1).

By changing the PrTMS ratio in the TMOS–PrTMS mixture, steric hindrance in the shell was controlled. To understand the effect of propyl groups in the shell, nitrogen adsorption–desorption isotherms were measured and the distributions of the pores were analyzed using the BJH method. Figure 1 shows the results for samples synthesized under different PrTMS ratio in the TMOS–PrTMS. Table 1 summarizes the properties of the samples. The isotherms are Type IV, which are similar to other MMSSs with or without organic functional groups.²⁶ The pore volume decreased as the co-condensation ratio of PrTMS ratio increased. The results are in qualitative agreement with the PrTMS ratio in the TMOS–PrTMS precursor. This behavior is similar to that of amino-functionalized MMSSs.²⁵

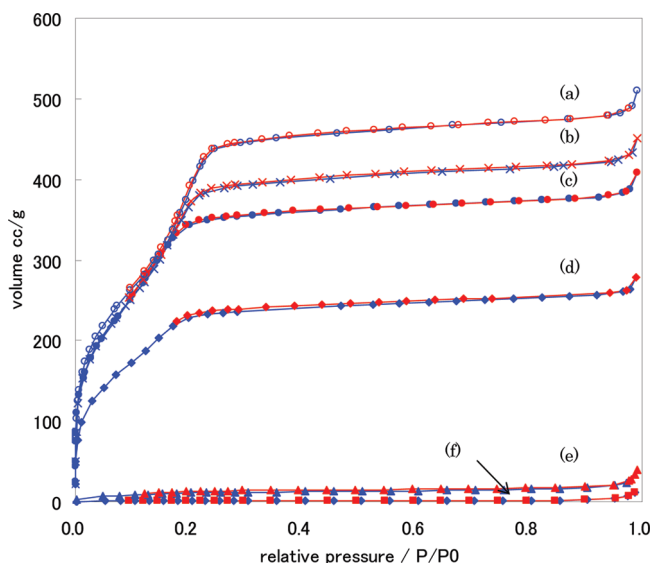


Figure 1. Nitrogen adsorption–desorption isotherms of (a) SH(10%)Pr(0%)(1), (b) SH(10%)Pr(10%)(1), (c) SH(10%)Pr(25%)(1), (d) SH(10%)Pr(50%)(1), (e) SH(10%)Pr(75%)(1), and (f) SH(10%)Pr(100%)(1).

The pore volume abruptly decreased and almost no nitrogen was adsorbed for SH(10%)Pr(75%)(1) and SH(10%)Pr(100%)(1). While the pore sizes of the SH(10%)Pr(75%)(1) and SH(10%)Pr(100%)(1) were larger, the values of the specific surface area and pore volume were the smallest. It is considered that organic functional groups of shell prevent the adsorption of nitrogen into the core. However, core/shell MMSSs that have thinner shells, such as SH(10%)Pr(75%)(1/2), SH(10%)Pr(75%)(1/4), and SH(10%)Pr(100%)(1/4), adsorbed a certain amount of nitrogen, although SH(10%)Pr(75%)(1) and SH(10%)Pr(100%)(1) hardly adsorbed N₂. This is expected to be enough to incorporate Au(III) ions into the pores of the mesoporous silica host.

To investigate the stability of the organic functional groups and reduction temperature of Au ions in the MMSS, thermogravimetric analysis (TG) of SH(10%)Pr(10%)(1) was measured in H₂(5%)/N₂ and O₂(20%)/N₂. (See Figure S2 in the Supporting Information.) In both cases, the MMSSs show similar weight loss (10 wt %) up to 240 °C. The MMSS experiences a weight loss of 7% upon heating up to 100 °C, which is likely due to water trapped inside, or adsorbed onto, the MMSS spheres. A difference between the two measurements is seen at the second stage of weight loss, at which point rapid weight loss due to the combustion of the organic moieties was seen in O₂(20%)/N₂ at 250 °C, but only a slow weight loss was seen up to 600 °C in H₂(5%)/N₂, under which conditions reduction of the Au ion is conducted. Based on the above results, it is assumed that the organic moieties are slowly lost after losing water molecules but still remained up to 250 °C. Thus, we conducted reduction experiments at <250 °C.

Au-Ion Loading. A series of Au–silica composite particles, SH(10%)Pr(*x*%)(*y*)Au were prepared in a manner similar to that recently reported procedure. After the immersion in HAuCl₄ solution, and the subsequent filtration,

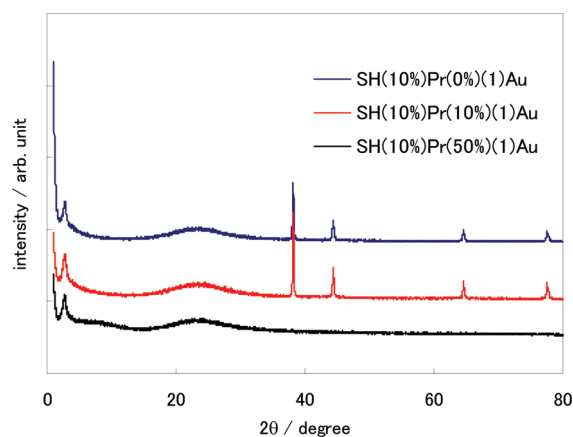


Figure 2. Powder X-ray diffraction (XRD) patterns of Au-loaded samples SH(10%)Pr(0%)(1)Au, SH(10%)Pr(10%)(1)Au, and SH(10%)Pr(50%)(1)Au.

pale yellow samples were obtained, which indicated the formation of Au-ion–MMSS complexes. Au amount determined from the EDX analysis on SEM were ca. 9.17 wt %, 8.51 wt %, and 0.87 wt %, for SH(10%)Pr(10%)(1)Au, SH(10%)Pr(50%)(1)Au, and SH(10%)Pr(75%)(1)Au, respectively. This result reveals that the high molar fraction of propyl groups of the shell prevent Au ions adsorbing into the core due to steric hindrance of the propyl group. This result is in agreement with the results obtained from nitrogen adsorption–desorption measurements. The gold amount of other Au–silica composite particles ranges from 11.78 wt % to 6.13 wt %. (See Table S1 in the Supporting Information.)

Figure 2 shows the powder XRD patterns of Au-loaded samples, SH(10%)Pr(0%)(1)Au, SH(10%)Pr(10%)(1)Au, and SH(10%)Pr(50%)(1)Au. SH(10%)Pr(0%)(1)Au and SH(10%)Pr(10%)(1)Au showed sharp peaks between 30° and 80°, whereas no peaks were seen for SH(10%)Pr(50%)(1)Au. The reflection obtained from the samples corresponds to the crystalline structure of gold. The peaks are assigned to the diffraction from the (111), (200), (220), and (311) planes of fcc gold, respectively. The appearance of sharp peaks is indicative of the generation of crystalline gold on the outer surface without heat treatment. This is confirmed by TEM analysis. (See Figure S3 in the Supporting Information.) It has been reported recently that the presence of water in the gold-precursor-loaded mesoporous silica causes the formation of spherical or almost-spherical gold nanoparticles, probably due to the large interface energy between gold and water, as evidenced by the easy formation of spherical gold nanoparticles in aqueous solutions.^{35–37} The gold precursor species are catalytically reduced at the pore surface so that the particles grow longer along the direction of the pore channels in the presence of water.³¹ In SH(10%)Pr(0%)(1)Au and

- (35) Fukuoka, A.; Higuchi, T.; Ohtake, T.; Oshio, T.; Kimura, J.; Sakamoto, Y.; Shimomura, N.; Inagaki, S.; Ichikawa, M. *Chem. Mater.* **2006**, *18*, 337.
 (36) *Colloidal Gold: Principles, Methods and Applications*; Handley, D. A., Ed.; Academic Press: San Diego, CA, 1989; Vol. 1.
 (37) Tsung, C. K.; Hong, W. B.; Shi, Q. H.; Kou, X. S.; Yeung, M. H.; Wang, J. F.; Stucky, G. D. *Adv. Funct. Mater.* **2006**, *16*, 2225.

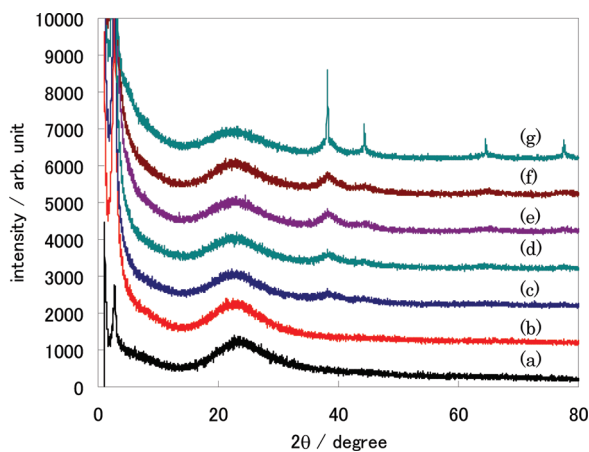


Figure 3. Powder XRD patterns of SH(10%)Pr(50%)(1)AuT after heat treatment at different temperature: (a) before heat treatment, (b) 100 °C, (c) 120 °C, (d) 150 °C, (e) 180 °C, (f) 200 °C, and (g) 230 °C.

SH(10%)Pr(10%)(1)Au, gold precursor species are reduced and grow in the mesopore and finally the gold particles migrate to the surface of the MMSSs. On the other hand, when the amount of the hydrophobic groups incorporated into the shell were increased, the number of water inside mesopores was decreased because of the increase of hydrophobic character and steric hindrance of organic groups inside the mesopores. Thus, the hydrophobic organic group in SH(10%)Pr(50%)(1) prevents migration of the gold precursor in the mesopores before heat treatment.

Reduction of Composites. Hydrogen reduction of the MMSSs impregnated with the gold precursor at different temperature produces gold nanoparticles of varying the size and number densities within the MMSSs. The ability to control the size and number densities of gold nanoparticles within the dielectric silica is expected to be important for the plasmonic and optoelectronic applications of the composite nanostructures.³⁷ To see the effect of the shell precisely in these composite materials, the amount of the shell and PrTMOS ratio in the shell were varied and XRD patterns were measured after heat treatment. First, SH(10%)Pr(50%)(*x*)AuT (where *x* = 1, 3/4, 1/2, 1/4; *T* = 120, 150, 180, 200, 230) were examined. Amounts of the TMOS–PrTMS mixture were decreased in this series. Figure 3 shows the XRD patterns of SH(10%)Pr(50%)(1)AuT after heat treatment at different temperature. Broad peaks are seen in the pattern, at 2θ between 30° and 80°, when the samples were heated above 120 °C, whereas no peaks, which correspond to crystalline gold, were seen below 100 °C. The reflection obtained from the samples corresponds to the crystalline structure of gold. This result is indicative of the beginning of crystalline gold growth, at ~120 °C. The intensity of the broad peaks gradually increased with increasing temperature. SH(10%)Pr(50%)(1)Au230 showed sharp peaks, which are indicative of the Au particle growth on the outer surface of MMSS. SH(10%)Pr(50%)(3/4)Au shows no sharp peaks in the XRD pattern up to 200 °C, which is similar to SH(10%)Pr(50%)(1)Au. (See Figure S4 in the Supporting Information.) On the other hand, SH(10%)Pr(50%)(1/2)Au

shows sharp peaks at 180 °C. (See Figure S5 in the Supporting Information.) This is due to the thin shell and may be caused by the thermal sintering to give crystalline gold on the surface of the MMSS at lower temperature. SH(10%)Pr(50%)(1/4)Au shows sharp peaks before heat treatment. This behavior is similar to that of SH(10%)Pr(0%)(1)Au and SH(10%)Pr(10%)(1)Au. Second, the molar ratio of PrTMOS in the shell was increased and the amount of additional TMOS–PrTMS mixture was decreased. SH(10%)Pr(75%)(1/2)Au, SH(10%)Pr(75%)(1/4)Au, and SH(10%)Pr(100%)(1/4)Au were examined. While the XRD patterns of SH(10%)Pr(75%)(1/2)AuT are similar to those of SH(10%)Pr(50%)(3/4)AuT and SH(10%)Pr(50%)(1)AuT up to 200 °C (see Figure S6 in the Supporting Information), SH(10%)Pr(75%)(1/4)Au shows sharp peaks in the XRD pattern at lower temperature. (See Figure S7 in the Supporting Information.) From these results, it can be concluded that more than 50 mol % of PrTMS and more than half the amount of silica species in the shell against the core are necessary to hold the crystalline gold in the MMSS mesopore after heat treatment.

TEM observations were performed to confirm the core/shell structures and gold particles in the core/shell MMSS. Figure 4 shows TEM images of SH(10%)Pr(50%)(1)AuT (*T* = 120 °C, 150 °C, 180 °C). An ovoid structure can be seen in Figure 4, indicating gold (the dark part of the images) was selectively adsorbed to the thiol-functionalized core and remained in the core after heat treatment. The thicknesses of the shells were estimated to be 56, 44, and 23 nm for SH(10%)Pr(50%)(1)Au, SH(10%)Pr(50%)(3/4)Au, and SH(10%)Pr(50%)(1/2)Au, respectively (see Figures S8 and S9 in the Supporting Information). The thickness of the shell was proportional to the amount of the additive silica source that was used. These values agreed well with the calculated values, from the silica precursors used for the core and shell synthesis. TEM images indicate that gold particles in samples after heat treatment have a particle size distribution ranging from single nanometer to ca. 15 nm. We have reported gold-nanoparticle-embedded MMSS samples that have no shell. Gold nanoparticles were found not only in the MMSS but also on the outer surface of the MMSS. On the other hand, gold particles were not seen on the outer surface of the core/shell MMSS and the gold nanoparticles were confined inside the core. Note that many gold nanoparticles were larger than the pore size (ca. 2 nm), indicating that the gold particles broke the silica pore walls to grow larger at temperatures of <200 °C. Similar phenomenon has been observed previously in the growth of gold nanoparticles inside mesoporous silicas.³⁷ It is considered that the wall thickness of ordered nanoporous silica is too thin to prevent the particle growth of gold during the reduction process, even at relatively low temperature (200 °C).³⁸

Figure 5 shows the diffuse reflectance spectra of the gold-nanoparticle-embedded MMSS samples, SH(10%)

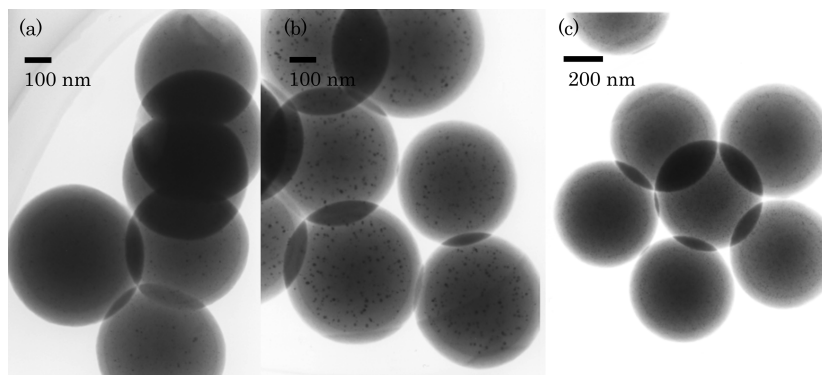


Figure 4. TEM images of SH(10%)Pr(50%)(1)AuT: (a) 120 °C, (b) 150 °C, and (c) 180 °C.

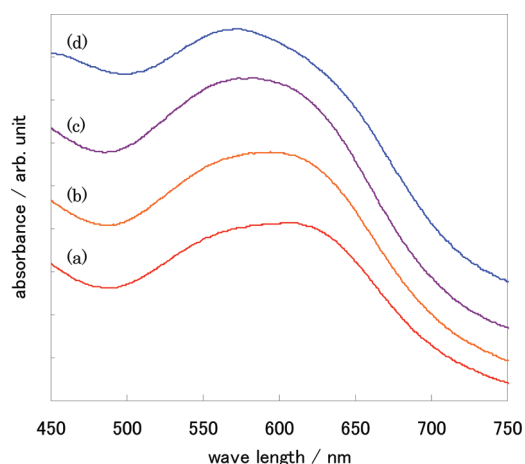


Figure 5. Diffuse reflectance spectra of SH(10%)Pr(50%)(1)AuT: (a) $T = 120$ °C, (b) $T = 150$ °C, (c) $T = 180$ °C, and (d) $T = 200$ °C.

Pr(50%)(1)AuT ($T = 120, 150, 180, 200$ °C) obtained at different heat treatment temperature. The spectrum of SH(10%)Pr(50%)(1)Au120 showed a peak and shoulder at ~ 604 and ~ 550 nm, respectively. The peak position of the spectrum shifted from 604 nm to 572 nm with increasing temperature from 120 °C to 200 °C. Figure 6 shows the shift of peak positions for the series of SH(10%)Pr(50%)(y)AuT. The behavior of diffuse reflectance spectra for SH(10%)Pr(75%)(1/2)AuT is similar to that of a series of SH(10%)Pr(50%)(y)AuT. (See Figure S10 in the Supporting Information.) The position and intensity of the gold surface-plasmon absorption band depends on the particle size and shape, the interaction between particles, and the optical and electronic properties of the medium surrounding the particles.³⁹ Although gold nanoparticles with sizes between single nanometer and ca. 15 nm does influence the position of the surface plasmon band, deviations from the spherical geometry, the medium surrounding, and the interaction between particles are much more relevant.⁴⁰ We assume that if the reduction temperature is lowered, the diameter of the gold nanoparticles become smaller, the number density of the gold nanoparticles within the MMSSs increases, and the absorption peak of the resulting composite move to

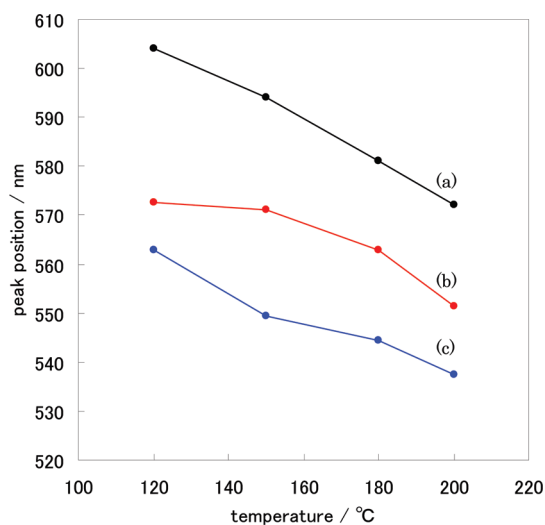


Figure 6. Plasmon peak positions of SH(10%)Pr(50%)(y)AuT: (a) $y = 1$, (b) $y = 3/4$, and (c) $y = 1/2$ after heat treatment at different temperature.

higher wavelength. A similar substantial shift of the absorption peak is found in mesoporous silica nanofibers.³⁷

It is known that plasmonic materials sometimes affect the emission of dyes. We conducted the experiment to confirm this phenomenon using Au-loaded MMSS samples. Preliminary results are shown in Figure S11 of the Supporting Information. An organic dye, Fluorol 555, was mixed with Au-loaded MMSSs in the solid state, and the emission spectra were collected. It was found that the maximum intensity of the emission of the dye changed depending the shell thickness of Au-loaded MMSS samples. However, to understand plasmonic behavior precisely, the effect of another factor, such as plasmon peak wavelength, also should be counted. Further studies are in progress to investigate the effect of plasmon resonance of gold nanoparticles.

Nitrogen adsorption measurements for SH(10%)Pr(50%)(3/4)Au150 and SH(10%)Pr(75%)(1/2)Au150 show that gold-nanoparticle-embedded samples are mesoporous material, with high surface area and pore volume. (See Figure S12 in the Supporting Information.) Smaller values can be observed for the SH(10%)Pr(50%)(3/4)Au150, with respect to the SH(10%)Pr(50%)(3/4); this is attributed to the presence of Au nanoparticles in the mesopores.

(39) Makarova, O. V.; Ostafin, A. E.; Miyoshi, H.; Norris, J. R.; Meisel, D. *J. Phys. Chem. B* **1999**, *103*, 9080.

(40) Liz-Marzan, L. M. *Langmuir* **2006**, *22*, 32.

Conclusion

In conclusion, we have synthesized a series of organically functionalized core/shell monodispersed mesoporous silica spheres (MMSSs) containing the bulky propyl group as a barrier in the shell and thiol groups as coordination sites of Au ions in the core. The thickness and molar ratio of propyl group of the shell are controlled by the amount of additional silica precursor and Au nanoparticles are retained within the core after heat treatment, because of the steric hindrance of the propyl group. The absorption maximum of the Au nanoparticles

showed a blue-shift not only with decreasing thickness of the shell but also with increasing reduction temperature. Because the gold-nanoparticle-embedded composites obtained herein still have large surface areas and pore volumes, a variety of nanoparticles, functional materials, and proteins (such as quantum dots, dyes, and enzymes) can be incorporated. They have potential applications in magneto-optical materials, drug delivery systems, catalysis, and novel plasmonic materials.

Supporting Information Available: Supporting Information is available free of charge via the Internet at <http://pubs.acs.org/>.